Migration velocity analysis in factorized VTI media

Debashish Sarkar & Ilya Tsvankin
Center for Wave Phenomena, Dept. of Geophysics, Colorado School of Mines

ABSTRACT

One of the main challenges in anisotropic velocity analysis and imaging is reliable estimation of both velocity gradients and anisotropic parameters from reflection data. Approximating the subsurface by a factorized VTI (transversely isotropic with a vertical symmetry axis) medium provides a convenient way of building vertically and laterally heterogeneous anisotropic models for prestack migration. The algorithm for P-wave migration velocity analysis (MVA) introduced here is designed for 2-D models composed of factorized VTI layers or blocks with constant vertical and lateral gradients in the vertical velocity V_{P0}. The anisotropic MVA method is implemented as an iterative two-step procedure that includes prestack depth migration (imaging step) followed by an update of the medium parameters (velocity-analysis step). The iterations for a particular block continue until the corresponding reflection events in image gathers are sufficiently flat. The residual moveout of the migrated events, which is needed to compute parameter updates, is described by a nonhyperbolic equation governed by two moveout parameters determined from semblance analysis.

For piecewise-factorized VTI media treated here, the residual moveout of P-wave events in image gathers is governed by four effective quantities in each block: (1) the normal-moveout (NMO) velocity $V_{\rm nmo}$ at a certain point within the block, (2) the vertical velocity gradient k_z, (3) the combination $\hat{k}_x = k_x\sqrt{1+2\delta}$ of the lateral velocity gradient k_x and the anisotropic parameter δ, and (4) the anellipticity parameter η. We show that all four parameters can be estimated from the residual moveout for at least two reflectors within a block and establish the minimum depth separation between the reflectors and the minimum lateral distance to be covered by the image gathers. Stable inversion for the parameter η also requires using either long-spread data (with the maximum offset-to-depth ratio no less than two) from horizontal interfaces or reflections from dipping interfaces.

To find the depth scale of the section and build a model for prestack depth migration using the MVA results, the vertical velocity V_{P0} needs to be specified for atleast a single point in each block. When no borehole information about V_{P0} is available, a well-focused image can often be obtained by assuming that the vertical-velocity field is continuous across layer boundaries. A synthetic test for a three-layer model with a syncline structure confirms the accuracy of our MVA algorithm in estimating the interval parameters $V_{\rm nmo}$, k_z, $\hat{k}_x$, and η and illustrates the influence of errors in the vertical velocity on the image quality.

1 INTRODUCTION

Most existing velocity-analysis methods for VTI (transversely isotropic with a vertical symmetry axis) media approximate the subsurface with homogeneous or vertically heterogeneous layers or blocks (e.g., Alkhalifah and Tsvankin, 1995; Le Stunff and Jeannot, 1998; Tsvankin, 2001; Grechka et al., 2002). Anisotropic layers, however, are often characterized by non-negligible lateral velocity gradients that may distort the shape of underlying reflectors and cause errors in the anisotropic parameters. Since lateral homogeneity is an inherent assumption in time imaging, whether isotropic or anisotropic, it is justified to ignore lateral gradients in the time-domain velocity analysis of P-waves in VTI media (e.g., Alkhalifah, 1997; Han et al., 2000). In contrast, anisotropic

depth imaging has to account properly for both vertical and lateral variations of the velocity field.

An analytic correction of normal-moveout (NMO) ellipses for lateral velocity variation in anisotropic media was developed by Grechka and Tsvankin (1999). Their method, however, is limited to horizontal layers, small lateral velocity gradients, and the hyperbolic portion of reflection moveout. Also, for purposes of depth imaging, we are interested in estimating lateral velocity variation rather than just removing its influence on anisotropic inversion. The main problem in reconstructing a spatially varying anisotropic velocity field is caused by the trade-offs between the velocity gradients, anisotropic parameters, and the shapes of the reflecting interfaces. Even in isotropic media, some trade-offs between the velocity field and reflector shapes cannot be resolved even in isotropic media without *a priori* information. A practical way to incorporate vertical and lateral velocity variations into anisotropic velocity analysis without excessively compromising the uniqueness of the solution is to adopt the so-called *factorized anisotropic model* in which the ratios of the stiffness coefficients (and, therefore, the anisotropic parameters) are constant.

Here, we consider a model composed of factorized VTI blocks, where each block is bounded by plane or irregular interfaces. The problem is treated in two dimensions, which implies that the vertical incidence plane that contains sources and receivers should coincide with the dip plane of the subsurface structure. The vertical P-wave velocity V_{P0} is assumed to vary linearly within each block, so the vertical (k_z) and lateral (k_x) gradients in V_{P0} are constant. The kinematics of P-wave propagation in each block can be described by five parameters: the velocity V_{P0} defined at a certain spatial location, the gradients k_z and k_x, and Thomsen (1986) anisotropic parameters ϵ and δ. Although it is possible to introduce jumps in velocity across the boundaries of the blocks, this model can be conveniently used to generate smooth velocity fields required by many migration algorithms (in particular, those based on ray tracing).

Since our goal is to estimate the relevant VTI parameters and carry out depth imaging for models with significant lateral and vertical velocity variation and considerable structural complexity, velocity model building is conveniently implemented in the prestack depth-migrated domain (e.g., Stork, 1991; Liu, 1997). Parameter estimation in the post-migrated domain, usually referred to as migration velocity analysis (MVA), consists of two main steps: (1) parameter update designed to minimize the residual moveout of events in the image gathers, and (2) prestack depth migration that creates an image of the subsurface using the updated parameters estimated in step (1). These two steps are iterated until the events in the image gathers are sufficiently flat. Note that MVA is quite robust in the presence of random noise because migration improves the signal-to-noise ratio (Gardner et. al., 1974; Liu, 1997).

The parameter-estimation methodology employed here is based on the results of Sarkar and Tsvankin (2002), hereafter referred to as *Paper I*. Although depth imaging of P-wave data requires knowledge of the five parameters listed above (V_{P0}, k_z, k_x, ϵ, and δ) in each block, Paper I shows that the moveout of events in image gathers is governed by the following four combinations of these parameters:
(1) the NMO velocity at a certain point on the surface of the factorized layer or block: $V_{\rm nmo} \equiv V_{P0}\sqrt{1+2\delta}$;
(2) the vertical velocity gradient k_z;
(3) the lateral velocity gradient combined with the parameter δ: $\hat{k}_x = k_x\sqrt{1+2\delta}$;
(4) the anellipticity parameter $\eta \equiv (\epsilon-\delta)/(1+2\delta)$.
If prestack migration is performed with the correct values of $V_{\rm nmo}$, k_z, $\hat{k}_x$, and η, the image gathers for reflections from both horizontal and dipping interfaces are flat. To decouple the horizontal gradient k_x from the coefficient δ and determine the other anisotropic coefficient ϵ, the velocity V_{P0} has to be known at a certain point within the factorized block (Paper I).

The paper starts with a discussion of the minimum information required to estimate the model parameters from P-wave moveout data. Then we give a description of the MVA methodology including nonhyperbolic moveout analysis on image gathers needed to constrain the anisotropic velocity field. The accuracy of the algorithm and its robustness in the presence of random noise are assessed by synthetic tests for a single layer and a multilayered factorized VTI medium. We also discuss different ways to specify the vertical velocity V_{P0} and the influence of errors in V_{P0} on the inverted values of the other parameters and on the quality of the migrated image.

2 PARAMETER ESTIMATION IN A FACTORIZED VTI LAYER

Here, we use the results of Paper I to evaluate the feasibility of estimating the parameters of a factorized VTI layer from P-wave reflection data. By replacing the actual factorized $v(x,z)$ model with narrow vertical strips of factorized $v(z)$ media, Paper I demonstrates that the moveout of a single horizontal event in an image gather is governed by the effective values of the NMO velocity and the parameter η:

$$v^2_{\rm nmo}(x,t_0) = V^2(x)(1+2\delta)\,\frac{e^{2k_z t_0}-1}{2k_z\,t_0}\,, \qquad (1)$$

$$\hat{\eta}(x,t_0) = \frac{1}{8}\left\{\frac{(1+8\eta)\,(e^{2k_z\,t_0}-1)\,k_z\,t_0}{2(e^{k_z t_0}-1)^2}+1\right\}; \qquad (2)$$

$V(x) \equiv V_{P0} + k_x\,x$ is the vertical P-wave velocity at the surface, and $t_0 \equiv t_0(x,z)$ is the zero-offset time at location x from a horizontal reflector at depth z.

If long-offset data needed to constrain $\hat{\eta}$ (Grechka

and Tsvankin, 1998) have been acquired, moveout analysis of a single event can yield estimates of both $v_{\rm nmo}(x,t_0)$ and $\hat{\eta}(x,t_0)$. Next, suppose that P-wave traveltimes from two horizontal reflectors sufficiently separated in depth are available. Then the ratio of the NMO velocities for these two events ($v_{\rm nmo,1}$ and $v_{\rm nmo,2}$) can be used to find [equation (1)]

$$\frac{v^2_{\rm nmo,1}(x,t_{0,1})}{v^2_{\rm nmo,2}(x,t_{0,2})} = \frac{t_{0,2}\,(e^{2k_z\,t_{0,1}}-1)}{t_{0,1}\,(e^{2k_z\,t_{0,2}}-1)}\,, \qquad (3)$$

where $t_{0,1}$ and $t_{0,2}$ are the zero-offset times for the two events. According to equation (3), conventional hyperbolic moveout analysis of two horizontal events located in the same factorized block can provide an estimate of the vertical gradient k_z. Knowledge of k_z and the zero-offset time t_0 is sufficient for obtaining the anellipticity parameter η from equation (2) applied to one or both reflection events. The remaining two key quantities, $V_{\rm nmo} = V_{P0}\sqrt{1+2\delta}$ and $\hat{k}_x = k_x\sqrt{1+2\delta}$, can then be computed from equation (1), if the effective NMO velocities are determined at two or more locations x.

We conclude that the moveout of horizontal events at two different depths and two image locations provides enough information to estimate the parameters $V_{\rm nmo}$, k_z, $\hat{k}_x$, and η. For the special case of a factorized $v(z)$ medium with a constant vertical gradient k_z, the moveouts of two horizontal events at a single image location can be inverted for the parameters $V_{\rm nmo}$, k_z, and η.

As shown in Paper I, reflection moveout of dipping events in factorized $v(x,z)$ VTI media is controlled by the same parameters ($V_{\rm nmo}$, k_z, $\hat{k}_x$, and η) as that of horizontal events. Most importantly, NMO velocity of events dipping at 25-30° or more is highly sensitive to the parameter η (Alkhalifah and Tsvankin, 1995; Tsvankin, 2001), whereas the inversion of nonhyperbolic moveout from horizontal reflectors for η may suffer from instability (Grechka and Tsvankin, 1998). Therefore, the inclusion of dipping events in velocity analysis is helpful in obtaining accurate estimates of η; also, dip-dependent reflection moveout provides additional information about the parameters $V_{\rm nmo}$, k_z, and $\hat{k}_x$.

Still, even if both horizontal and dipping events are available, the parameters V_{P0}, k_x, ϵ, and δ remain generally unconstrained by P-wave reflection traveltimes. In particular, the vertical velocity V_{P0} is needed to define the depth scale of the VTI model in the migration of P-wave data. Hence, to build an anisotropic model for depth imaging, at least one medium parameter must be known *a priori*. Unless specified otherwise in the synthetic data examples discussed below, the velocity V_{P0} is assumed known at some location on the surface of each factorized layer. Given this information about V_{P0}, we can use velocity analysis of P-wave data to estimate the parameters k_z, k_x, ϵ, and δ.

3 ALGORITHM FOR MIGRATION VELOCITY ANALYSIS

Inversion of seismic data is a nonlinear problem that can be solved through an iterative application of migration and velocity updating. Migration creates an image of the subsurface for trial values of the medium parameters, and then velocity analysis is used to update the model for the next run of the migration code. This iterative procedure, conventionally called *migration velocity analysis* (MVA), is continued until a certain criterion (e.g., small residual moveout of events in image gathers) is satisfied.

Here, we apply anisotropic prestack depth migration (the migration algorithm is described in detail in Paper I) and tomographic velocity update to P-wave data acquired over the subsurface composed of factorized $v(x,z)$ VTI blocks. The iterations are stopped when the residual moveout for at least two reflectors in each factorized block is close to zero (i.e., the migrated depth stays the same to within a specified fraction of the wavelength for different offsets). The overall organization of our MVA algorithm is similar to that developed by Liu (1997) for isotropic media, but the VTI model is characterized, for P-waves, by two additional parameters – ϵ and δ.

The tomographic update of the medium parameters is based entirely on the residual moveout of events in image gathers. For horizontal reflectors embedded in a weakly anisotropic homogeneous VTI medium, the migrated depth $z_{_M}$ in image gathers can be written as (Paper I):

$$z^2_{_M}(h) \approx z^2_{_M}(0) + h^2 V^2_{P0,M}\left(\frac{1}{V^2_{\rm nmo,}T} - \frac{1}{V^2_{\rm nmo,}M}\right) + \frac{2h^4}{h^2+z^2_{_T}}\left(\eta_{_M}\frac{V^2_{\rm nmo,}T}{V^2_{\rm nmo,}M} - \eta_{_T}\frac{V^2_{\rm nmo,}M}{V^2_{\rm nmo,}T}\right), \qquad (4)$$

where the subscripts T and M denotes the true and migration medium parameters, respectively, h is the half-offset, and $z_{_T}$ is the true zero-offset depth of the reflector. Equation (4) is nonhyperbolic and governed by two independent parameters – $V_{\rm nmo}$ and η. The NMO velocity $V_{\rm nmo}$ controls the hyperbolic (described by the h^2–term) part of the moveout curve and also contributes to the nonhyperbolic (h^4) term, while η influences nonhyperbolic moveout only. A similar closed-form expression is not available for dipping reflectors, but both the hyperbolic and nonhyperbolic portions of the residual moveout curve for dipping events also depend on $V_{\rm nmo}$ and η (Paper I).

As discussed above, the residual moveout of P-waves in factorized $v(x,z)$ VTI media is a function of the parameters $V_{\rm nmo}$, k_z, $\hat{k}_x$, and η. Although it is difficult to express the migrated depth $z_{_M}$ in laterally heterogeneous media analytically in terms of these parameters, the residual moveout equation can be cast in a form

similar to that in equation (4):

$$z_{M}^{2}(h) \approx z_{M}^{2}(0) + \mathrm{A}\,h^{2} + \mathrm{B}\,\frac{2h^{4}}{h^{2} + z_{M}^{2}(0)}\,. \qquad (5)$$

A and B are dimensionless constants that describe the hyperbolic and nonhyperbolic portions of the moveout curve, respectively. Numerical tests (see below) confirm that the functional form in equation (5) with fitted coefficients A and B provides a good approximation for P-wave moveout in long-spread image gathers.

To apply equation (5) in velocity analysis, we first pick an approximate value of the zero-offset reflector depth $z_{M}(0)$ on the migrated stacked section. The parameters A and B are obtained by a 2-D semblance scan on image gathers at each migrated zero-offset depth point. The best-fit combination of A and B that maximizes the semblance value is substituted into equation (5) to describe the residual moveout. It should be emphasized that the coefficients A and B in our algorithm are not directly inverted for the parameters V_{nmo}, k_z, $\hat{k}_x$, and η. Rather, the only role of A and B is in providing an adequate functional approximation for the residual moveout.

After estimating the residual moveout in image gathers, we update the N-element parameter vector $\boldsymbol{\lambda}$ using the algorithm described in Appendix A. The update $\boldsymbol{\Delta\lambda}$ of the parameter vector is obtained by solving the system of linear equations,

$$\boldsymbol{A^{T}\,A\,\Delta\lambda} = \boldsymbol{A^{T}\,b}\,. \qquad (6)$$

Here $\boldsymbol{A}$ is a matrix with $M \cdot P$ rows (P is the total number of image gathers used in the velocity analysis and M is the number of offsets) and N columns that includes the derivatives of the migrated depth with respect to the medium parameters. The superscript T denotes the transpose, and $\boldsymbol{b}$ contains the migrated depths that define the residual moveout. The full definitions of the matrix $\boldsymbol{A}$ and vector $\boldsymbol{b}$ are given in Appendix A.

For all examples described below, each iteration of the MVA consists of the following four steps:
(1) prestack depth migration with a given estimate of the medium parameters;
(2) picking along two reflectors in each VTI block to delineate the reflector shapes;
(3) semblance scanning using equation (5) to estimate A and B for image points along each reflector;
(4) application of equation (6) to update the medium parameters in such a way that the variance of the migrated depths as a function of offset is minimized (see Appendix A for more details about the minimization procedure).

Steps 1–4 are repeated until the magnitude of residual moveout of events in image gathers becomes sufficiently small.

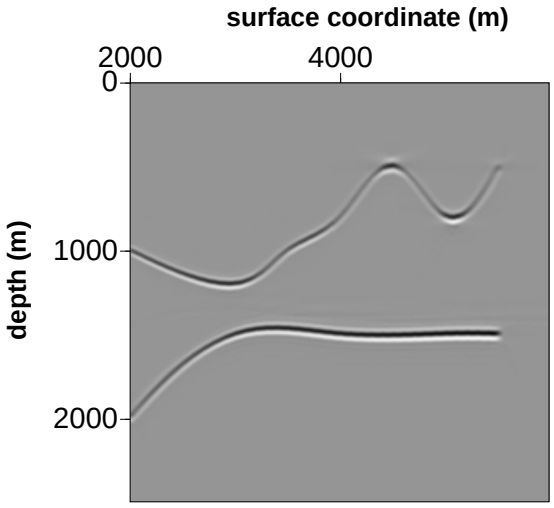

Figure 1. True image of two reflectors embedded in a factorized $v(x,z)$ VTI medium with the parameters $V_{P0}(x = 3\,\mathrm{km}, z = 0) = 2600$ m/s, $k_z = 0.6$ s^{-1}, $k_x = 0.2$ s^{-1}, $\epsilon = 0.1$, and $\delta = -0.1$. The corresponding effective parameters are $V_{\mathrm{nmo}}(x = 3\,\mathrm{km}, z = 0) = 2326$ m/s, $k_z = 0.6$ s^{-1}, $\hat{k}_x = 0.18$ s^{-1}, and $\eta = 0.25$.

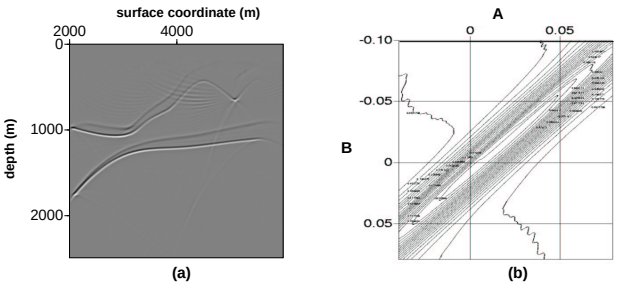

Figure 2. (a) Image of the model from Figure 1 obtained using a homogeneous isotropic velocity field with $V_{P0} = 2600$ m/s. (b) Semblance contour plot computed from equation (5) for the shallow reflector at the surface location 3 km.

4 EXAMPLE WITH A SINGLE FACTORIZED LAYER

First, we consider two irregular reflectors embedded in a factorized $v(x,z)$ VTI medium with $k_z > k_x > 0$ and a positive value of η typical for shale formations (Figure 1). For the first application of prestack depth migration, we choose a homogeneous, isotropic medium ($V_{P0} = 2600$ m/s, $k_z = k_x = \epsilon = \delta = 0$) as the initial velocity model. The migrated stacked image in Figure 2a is clearly inferior to the true image in Figure 1. We start the velocity-updating process by manually picking along both imaged reflectors to outline their shapes. Then

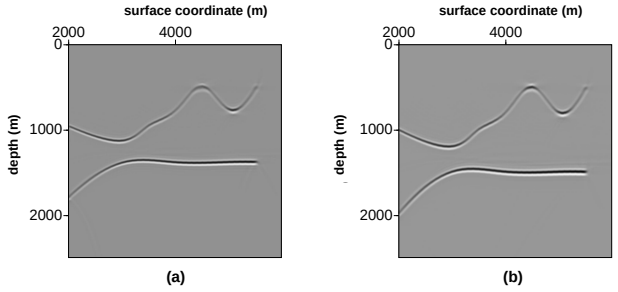

Figure 3. Stacked image after (a) four iterations; (b) eight iterations.

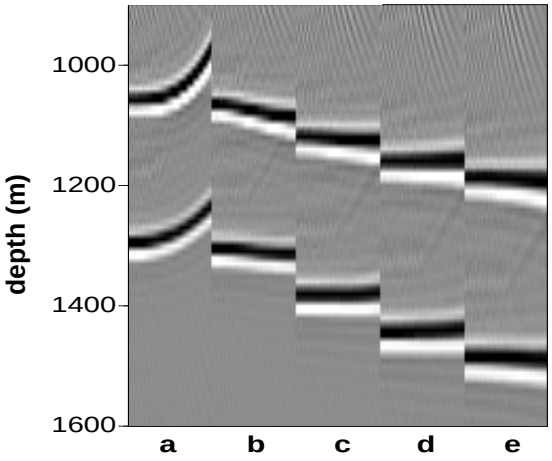

Figure 4. Residual moveout in image gathers for both reflectors at the surface location 3 km: (a) for the initial model; (b) after two, (c) four, (d) six, and (e) eight iterations. The residual moveout is minimized during the velocity-updating process.

equation (5) is used to compute two-parameter semblance scans for each reflector and evaluate the residual moveout in the image gathers.

One such semblance scan computed for the shallow reflector at the surface coordinate 3 km is displayed in Figure 2b. The values of A and B that correspond to the maximum semblance coefficient in Figure 2b provide an accurate description of residual moveout at this location. Although a certain degree of trade-off exists between A and B, any pair of values inside the innermost semblance contour gives almost the same variance of the migrated depths. Note that the interplay between A and B is similar to that between the NMO velocity and parameter η in the inversion of P-wave nonhyperbolic reflection moveout (Grechka and Tsvankin, 1998; Tsvankin, 2001).

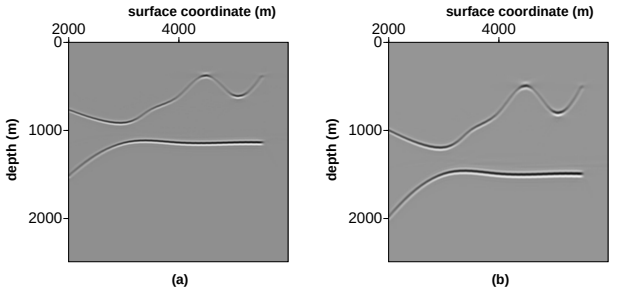

Figure 5. (a) Stacked image obtained after velocity analysis with the wrong value of the vertical velocity $V_{P0}(x = 3\,\text{km}, z = 0) = 2000$ m/s. The estimated medium parameters are $k_z = 0.58 \pm 0.02\ ^{-1}$, $k_x = 0.15 \pm 0.0\ \text{s}^{-1}$, $\epsilon = 0.51 \pm 0.0$, $\delta = 0.17 \pm 0.01$. (b) Stacked image for the correct medium parameters (Figure 1). Since V_{P0} in section (a) is smaller than the true value, both reflectors are shifted up with respect to their correct positions in section (b).

For purposes of velocity analysis, we use the image gathers at 12 equally spaced surface locations between 3 km and 4.2 km. The maximum offset-to-depth ratio for the selected image gathers at the shallow reflector is close to two, which is marginally suitable for estimating the parameter η. Tighter constraints on η are provided by the NMO velocities of reflections from the dipping segments of the shallow reflector (the dips exceed 30° in the middle of the section).

After the residual moveout has been evaluated, we fix the vertical velocity $V_{P0}(x = 3000\,\text{m}, z = 0) = 2600$ m/s at the correct value and update the parameters k_z, k_x, ϵ, and δ using equation (6). The stacked images after four (Figure 3a) and eight (Figure 3b) iterations illustrate the improvements in the focusing and positioning of both reflectors during the velocity update. The magnitude of the residual moveout for both reflectors decreases as the model parameters converge toward their actual values (Figure 4). The velocity-updating procedure is stopped after eight iterations because events in all analyzed image gathers are practically flat.

The inverted model parameters are close to the correct values: $k_z = 0.58 \pm 0.02\ \text{s}^{-1}$, $k_x = 0.2 \pm 0.0\ \text{s}^{-1}$, $\epsilon = 0.12 \pm 0.01$, and $\delta = -0.09 \pm 0.01$. The error bars were computed by assuming a standard deviation of ± 5 m in picking migrated depths on the selected image gathers and substituting this picking error into equation (6) to find the corresponding deviations of the model parameters near the actual solution.

The accurate results of the above test were obtained with the correct value of the vertical velocity at a given point on the surface of the factorized layer. Next, we apply the MVA method with an erroneous value of $V_{P0}(x = 3\,\text{km}, z = 0) = 2000\,\text{m/s}$, which is 23% smaller than the true velocity (2600 m/s). The stacked images of both reflectors obtained after the velocity analysis (Figure 5a) are well focused, which indicates that the im-

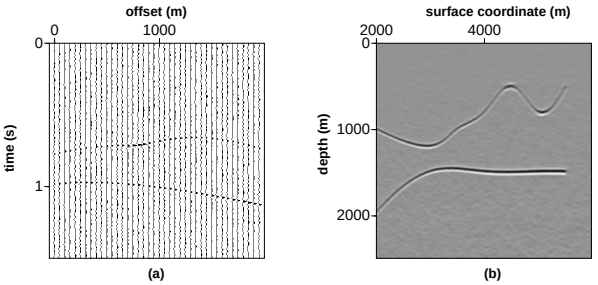

Figure 6. Influence of noise on the velocity analysis and migration. (a) A shot gather from the dataset in Figure 1 after the addition of Gaussian noise; the signal-to-noise ratio is 1.5. (b) The image obtained for the noisy dataset.

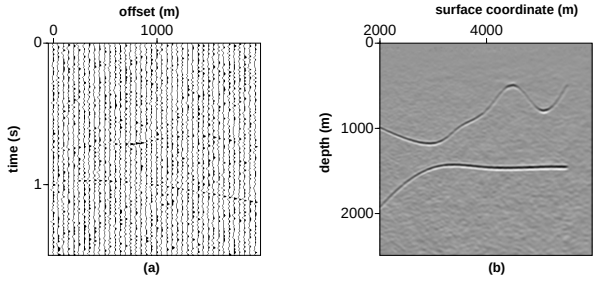

Figure 7. Influence of noise on the velocity analysis and migration. (a) The same shot gather as in Figure 6, but with a more severe noise contamination (signal-to-noise ratio is 1). (b) The image obtained for the noisy dataset.

age gathers have been flattened. Indeed, although the estimated medium parameters listed in the caption of Figure 5 are distorted, the effective parameters responsible for the residual moveout are close to their actual values: $V_{\rm nmo}(x = 3\,{\rm km}, z = 0) = 2315$ m/s, $k_z = 0.58$ s^{-1}, $\hat{k}_x = 0.17$ s^{-1}, and $\eta = 0.25$.

This result corroborates the analysis of residual moveout in Paper I and confirms that our algorithm converges toward the correct parameters $V_{\rm nmo}$, k_z, $\hat{k}_x$, and η, even if the vertical velocity V_{P0} on the surface of the layer is poorly known. Since V_{P0} assumed in the velocity analysis is too low, however, both reflectors in Figure 5a are imaged at depths that are about 23% smaller than the actual ones in Figure 5b. The depth distortion also leads to the rotation of the dipping segments of the reflecting interfaces, which is discussed in more detail below.

5 MVA IN THE PRESENCE OF NOISE

To evaluate the influence of noise on the estimation of the medium parameters and the quality of imaging, we added Gaussian noise to the data set from Figure 1. The signal-to-noise ratio, measured as the ratio of the peak amplitude of the signal to the root-mean-square (rms) amplitude of the background noise, is about 1.5, and the frequency bands of the noise and signal are identical (Figure 6a). The estimates of the medium parameters obtained after the migration velocity analysis with the correct value of V_{P0} at the surface location 3 km are as follows: $k_z = 0.56 \pm 0.04$ s^{-1}, $k_x = 0.2 \pm 0.0$ s^{-1}, $\epsilon = 0.12 \pm 0.02$, and $\delta = -0.09 \pm 0.02$. The error bars were computed in the same way as those for the noise-free synthetic example above (Figure 3), but the depth-picking error for all offsets and image locations was assumed to be 15 m instead of 5 m. Clearly, the noise contamination did not cause measurable errors in the medium parameters or noticeable distortions in the stacked image (Figure 6b).

Even for the much more severely contaminated data set in Figure 7, the inverted medium parameters are close to the actual values: $k_z = 0.52 \pm 0.07$ s^{-1}, $k_x = 0.2 \pm 0.01$ s^{-1}, $\epsilon = 0.13 \pm 0.03$, and $\delta = -0.07 \pm 0.03$, Here the error bars were computed under the assumption that the noise increased the depth-picking error to 20 m. (Since the dominant wavelength in this example was about 80 m, picking errors are unlikely to exceed 20 m, even for a substantial level of noise.) Also, despite the low signal-to-noise ratio, the migrated stacked section in Figure 7b has a sufficiently high quality, comparable to that of the true image in Figure 1.

We conclude that, the migration velocity analysis employed here gives reliable estimates of the anisotropic parameters and velocity gradients in the presence of random noise. One aiding factor is that the MVA operates on migrated data, which have a higher signal-to-noise ratio than do those of the original records because of partial stacking applied to the data during the migration step. The semblance (coherency) operator used to evaluate the residual moveout on image gathers also contributes to the robustness of the parameter estimation by suppressing remaining random noise in the migrated data.

6 SENSITIVITY STUDY

The above results demonstrate that, in principle, the residual moveout from two reflectors in a factorized layer is sufficient to estimate the four key parameters $V_{\rm nmo}$, k_z, $\hat{k}_x$, and η. This section is devoted to two important practical issues related to the implementation of our algorithm. By performing a series of numerical tests, we establish the minimum depth separation between the two reflectors and the minimum lateral spread of the image gathers (i.e., the difference between the largest and smallest surface coordinates of the image locations) needed for stable parameter estimation.

Consider two horizontal reflectors embedded in the factorized $v(x, z)$ medium with the parameters listed in

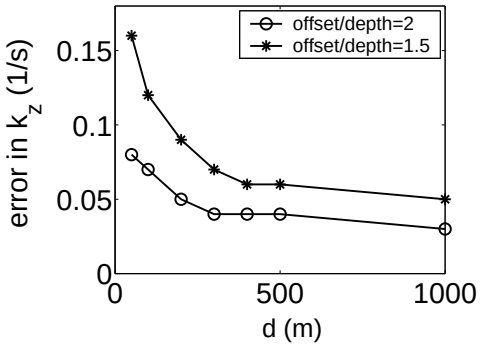

Figure 8. Influence of the vertical distance d between the two horizontal reflectors used in the velocity analysis on the absolute error in the vertical gradient k_z. The depth of the shallow reflector is 1 km; the maximum offset is 2 km for the upper curve and 1.5 km for the lower curve. The model parameters are $V_{P0}(x = 3\,\text{km}, z = 0) = 2600$ m/s, $k_z = 0.6$ s^{-1}, $k_x = 0.2$ s^{-1}, $\epsilon = 0.2$, and $\delta = 0.1$.

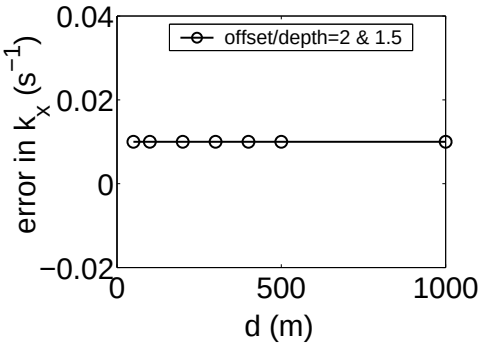

Figure 9. Influence of the distance between the two horizontal reflectors on the absolute error in the horizontal gradient k_x. The parameters are the same as in Figure 8.

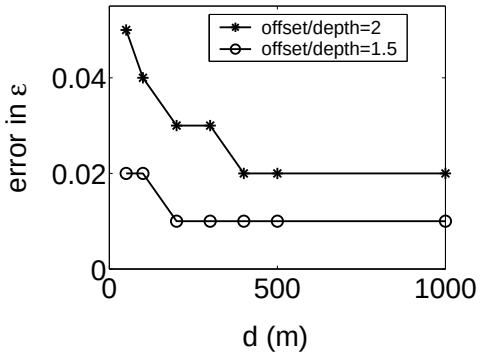

Figure 10. Influence of the distance between the two horizontal reflectors on the absolute error in the parameter ϵ. The parameters are the same as in Figure 8.

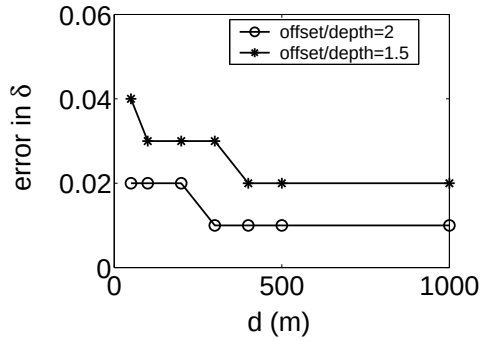

Figure 11. Influence of the distance between the two horizontal reflectors on the absolute error in the parameter δ. The parameters are the same as in Figure 8.

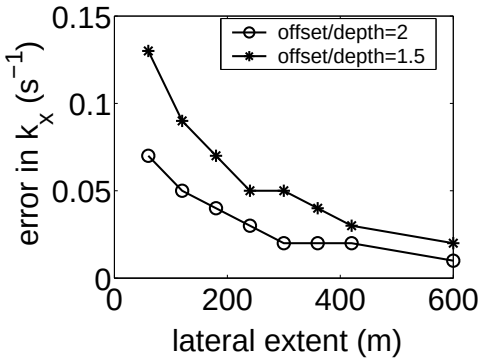

Figure 12. Influence of the lateral spread of the image gathers on the absolute error in k_x. The reflector depths are 1 km and 1.2 km; the other parameters are the same as in Figure 10. The velocity analysis is performed on 12 image gathers, each with 20 offsets.

the caption of Figure 8. The depth of the shallow reflector is fixed at 1000 m, while the depth of the second reflector varies from 1050 m to 2000 m. Figures 8–9 illustrate the dependence of the error in the estimated parameters k_z, k_x, ϵ, and δ on the distance between the reflectors. The errors in the parameters were computed from equation (6) assuming that the error in picking the migrated depths is ± 5 m. The velocity analysis operated with the residual moveout on 12 image gathers (with 20 offsets each) whose horizontal coordinates span a distance of 1200 m. For all tests, the vertical velocity at one location on the surface was held at the correct value.

For the parameters k_z, ϵ and δ, the dependence of the estimated error on the distance d between the reflectors has a similar character (Figures 8, 10, and 11). The error initially decreases rapidly with increasing d and then becomes almost constant as d approaches 500 m. For a maximum offset-to-depth ratio (at the shallow reflector) of two, the error curves flatten out for $d \approx 250$ m, which is equal to 1/5 of the depth of the bottom re-

flector. If the maximum offset-to-depth ratio is 1.5, the curve flattens out for a larger depth $d \approx 350$ m ($\approx$1/4 of the depth of the bottom reflector).

This behavior of the error curves is in good agreement with the analysis of the effective NMO velocity and parameter η in Paper I. Accurate estimation fo the vertical gradient k_z, and then the NMO velocity at the surface of the factorized layer, requires a sufficiently large difference between the NMO velocities of the two events used in the velocity analysis [see equation (3)]. In other words, the reflectors should be sufficiently separated in depth to resolve the interval NMO velocity, which carries information about the gradient k_z. An accurate estimate of k_z makes it possible to obtain $V_{\rm nmo}$ at the surface and then, using the nonhyperbolic portion of the moveout curve, the parameter η. The minimum suitable vertical distance d found here is close to the minimum layer thickness conventionally assumed in interval velocity estimation based on the Dix equation.

In contrast, the error in the horizontal gradient k_x is practically insensitive to variations in the distance between the two reflectors (Figure 9) because the lateral spread of the coordinates of the image gathers is kept constant at 1.2 km. The influence of the maximum horizontal distance between the image gathers on the error in k_x is shown in Figure 12. As expected, the gradient k_x becomes better constrained with increasing lateral spread of the image gathers, with the error curve flattening out for spreads exceeding 300-400 m.

Note that the errors in all parameters reduce with increasing number of offsets in the image gathers, which can influence the sensitivity estimates. Although the results of the error analysis also depend on the anisotropic coefficients ϵ and δ and the velocity gradients, this dependence is not significant if the velocity update is performed with reasonable constraints on the model parameters.

7 TEST FOR A MULTILAYERED MODEL

After performing a series of tests for a single factorized layer, we apply the algorithm to a three-layer model shown in Figure 13. Each layer contains two reflecting interfaces, as requried in our method, with every second reflector serving as the boundary between layers. The first and third layers are vertically heterogeneous [$v(z)$] and isotropic, while the second layer is a factorized, laterally heterogeneous [$v(x, z)$] medium. All interfaces are quasi-horizontal, with the largest dips (at the flanks of the syncline) of 10° or less. The model is designed to represent a typical depositional environment in the Gulf of Mexico, where anisotropic shale layers (the middle layer in Figure 13) are often embedded between isotropic sands.

For the velocity analysis we use image gathers located along the left flank of the syncline with the surface coordinates ranging from 4400 m to 5600 m; the maximum offset-to-depth ratio for the image gathers is close to two. The medium parameters are estimated in the layer-stripping mode starting at the surface. For the first (top) layer, the vertical velocity is assumed to be known at a single surface location [$V_{P0}(x = 4000\,\text{m}, z = 0\,\text{m}) = 1500$ m/s]. The chosen value of V_{P0} corresponds to that for water-bottom sediments; on land, V_{P0} at the

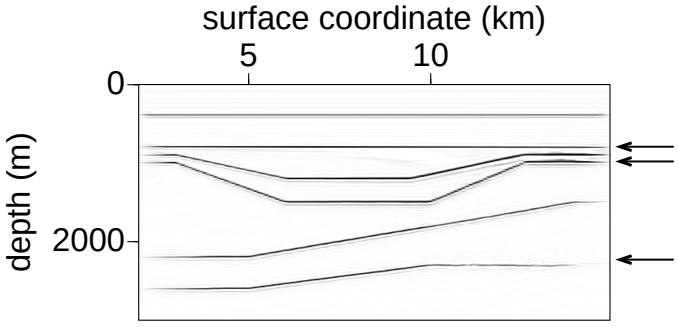

Figure 13. True image of a three-layer factorized medium. Every second reflector (indicated here with arrows) represents the bottom of a layer. The parameters of the first subsurface layer are $V_{P0}(x = 4000\,\text{m}, z = 0\,\text{m}) = 1500$ m/s, $k_z = 1.0\ \text{s}^{-1}$, and $k_x = \epsilon = \delta = 0$; for the second layer, $V_{P0}(x = 4000\,\text{m}, z = 800\,\text{m}) = 2300$ m/s, $k_z = 0.6\ \text{s}^{-1}$, $k_x = 0.1\ \text{s}^{-1}$, $\epsilon = 0.1$, and $\delta = -0.1$; for the third layer, $V_{P0}(x = 4000\,\text{m}, z = 1162\,\text{m}) = 2718$ m/s, $k_z = 0.3\ \text{s}^{-1}$, and $k_x = \epsilon = \delta = 0$.

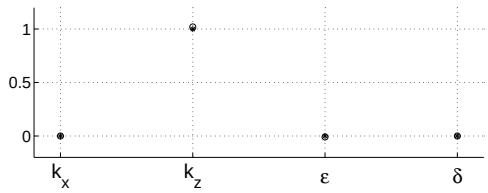

Figure 14. Estimated (○) and true (⋆) parameters of the first layer obtained using the correct $V_{P0}(x = 4000\,\text{m}, z = 0\,\text{m}) = 1500$ m/s on the surface.

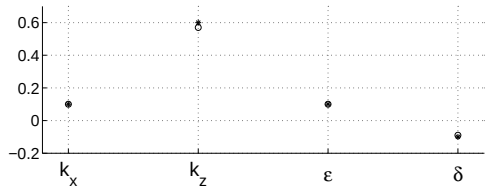

Figure 15. Estimated (○) and true (⋆) parameters of the second layer obtained using the correct $V_{P0}(x = 4000\,\text{m}, z = 800\,\text{m}) = 2300$ m/s at the layer's top.

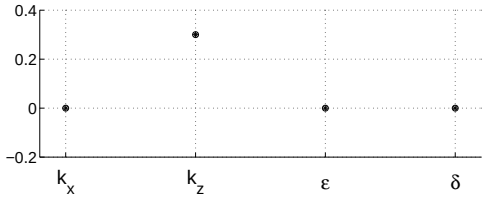

Figure 16. Estimated (∘) and true (⋆) parameters of the third layer obtained using the correct $V_{P0}(x = 4000\,\text{m}, z = 1162\,\text{m}) = 2718$ m/s at the layer's top.

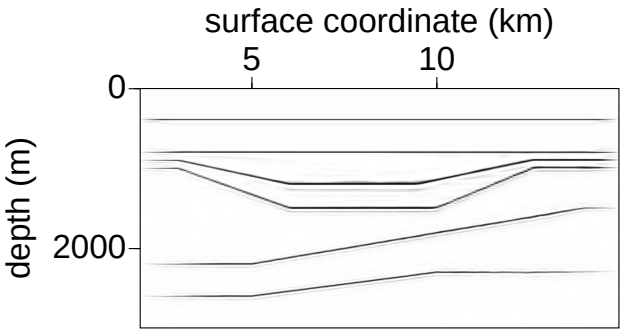

Figure 17. Stacked image obtained after prestack depth migration using the estimated parameters from Figures 14–16. The vertical velocity V_{P0} at the top of each layer was known.

top of the model may be estimated from near-surface velocity measurements. Starting with a homogeneous isotropic model ($V_{P0} = 1500$ m/s) the parameters k_z, k_x, ϵ, and δ in the first layer, obtained from the migration velocity analysis with the correct vertical velocity $V_{P0}(x = 4000\,\text{m}, z = 0\,\text{m})$, are close to the true values (Figure 14).

To estimate the medium parameters in the second and third layers, we need to fix the vertical velocity at a certain spatial location in each layer. Three different scenarios for choosing V_{P0} in the second and third layers are examined below.

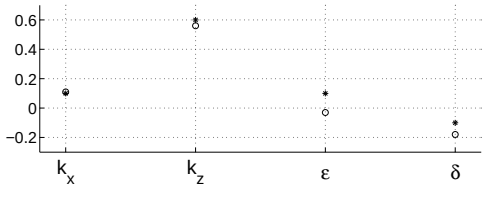

Figure 18. Estimated (∘) and true (⋆) parameters of the second layer obtained with an inaccurate value of the vertical velocity at the top of the second layer $[V_{P0}(x = 4000\,\text{m}, z = 800\,\text{m}) = 2600$ m/s].

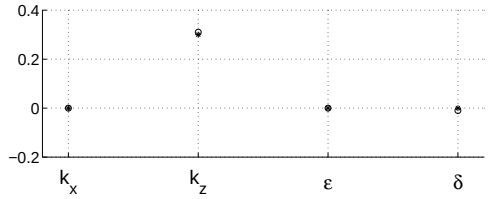

Figure 19. Estimated (∘) and the true (⋆) parameters of the third layer obtained with an inaccurate value of the vertical velocity at the top of the second layer $[V_{P0}(x = 4000\,\text{m}, z = 800\,\text{m}) = 2600$ m/s] but the correct $V_{P0}(x = 4000\,\text{m}, z = 1208\,\text{m}) = 2732$ m/s at the top of the third layer.

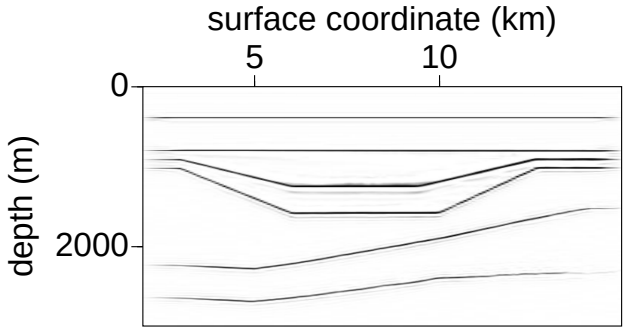

Figure 20. Stacked image obtained after prestack depth migration using the estimated parameters from Figures 14, 18, and 19. The vertical velocity V_{P0} at the top of the second layer was inaccurate.

7.1 V_{P0} at the top of each layer is known

Suppose a vertical borehole was drilled at the surface location 4000 m, and the vertical velocity at the top of the second and third layers was measured from sonic logs or check shots. Prestack depth migration with the estimated parameters of the first layer yields the depth of the top of the second layer at the surface location 4000 m. Using the correct value of the vertical velocity at this point $V_{P0}(x = 4000\,\text{m}, z = 800\,\text{m}) = 2300$ m/s,

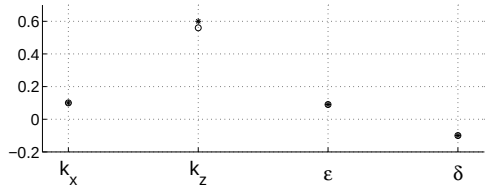

Figure 21. Estimated (∘) and true (⋆) parameters of the second layer obtained assuming that V_{P0} is continuous between the first and second layers at the point $(x = 3900\,\text{m}, z = 800\,\text{m})$.

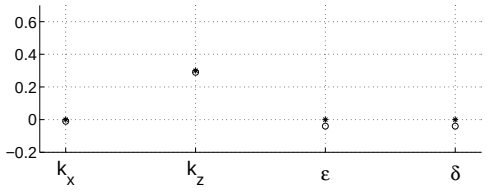

Figure 22. Estimated (○) and true (⋆) parameters of the third layer obtained assuming that V_{P0} is continuous between the first and second layers at the point ($x = 3900\,\text{m}, z = 800\,\text{m}$) and between the second and third layers at the point ($x = 5937\,\text{m}, z = 1483\,\text{m}$).

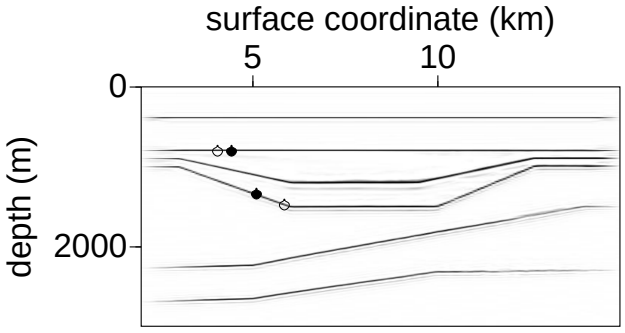

Figure 23. Stacked image obtained after prestack depth migration using the estimated parameters from Figures 14, 21, and 22. The vertical velocity was assumed to be continuous between the first and second layers at the point ($x = 3900\,\text{m}, z = 800\,\text{m}$) and between the second and third layers at the point ($x = 5937\,\text{m}, z = 1483\,\text{m}$). True (•) and estimated (○) points of continuity are also indicated.

we carry out the velocity analysis for the second layer, which results in good estimates of all four parameters (Figure 15). Repeating the same procedure for the third layer with the velocity $V_{P0}(x = 4000\,\text{m}, z = 1162\,\text{m}) = 2718$ m/s, we obtain the interval parameters close to the true values (Figure 16).

The shapes and depths of the reflectors imaged for the reconstructed velocity model (Figure 17) closely resemble those on the true image (Figure 13). This test confirms that migration velocity analysis in layered factorized VTI $v(x, z)$ media can be used to invert for the the velocity gradients k_z and k_x and the anisotropic coefficients ϵ and δ if the vertical velocity is known at a single point in each layer.

7.2 V_{P0} in the second layer is incorrect

Now suppose that the vertical velocity $V_{P0}(x = 4000\,\text{m}, z = 800\,\text{m})$ used for the top of the second layer has error (2600 m/s instead of 2300 m/s). Although this error in V_{P0} causes distortions in the inverted values of the other parameters (Figure 18), the effective quantities $V_{\text{nmo}}(x = 4000\,\text{m}, z = 800\,\text{m}) = 2080$ m/s, $k_z = 0.56\,\text{s}^{-1}$, $\hat{k}_x = 0.09\,\text{s}^{-1}$, and $\eta = 0.23$ do not significantly differ from the true values, which corroborates our results for a single layer (Figure 5). Since the assumed value of $V_{P0}(x = 4000\,\text{m}, z = 800\,\text{m})$ is higher than the correct velocity, the second layer is stretched in depth by about 13%, and the bottom of the syncline is imaged at a depth that is 80m too large (Figure 20). This depth stretch in the second layer also causes a tilt of the syncline's flanks whose dips in Figure 20 exceed the true values.

To continue the velocity analysis, we fix the vertical velocity at the imaged top of the third layer at the correct value. Despite the depth shift of the top of the third layer, the algorithm yields accurate values of all four interval parameters (Figure 19).Because of the depth and dip distortions in the second layer, however, the two bottom reflectors are imaged at somewhat greater depths and are slightly deformed (Figure 20). In particular, on the left side of the section the fifth and sixth reflectors are no longer horizontal; they have acquired mild dips to conform to the stretched synclinal structure above.

7.3 V_{P0} is continuous across the boundaries

If no borehole information is available, one assumption that might be made is that the velocity V_{P0} is a continuous function of depth at a certain horizontal coordinate. To identify this point of continuity at the boundary between the first and second layers, we examine the moveout along the third and fourth reflectors (only for offsets smaller than 1000 m) after migration with an isotropic homogeneous velocity field in the second layer. The migration velocity was chosen to be equal to the estimated velocity at the bottom of the first layer (i.e., at the second reflector). To select the point of continuity, we pick the surface coordinate with the smallest residual moveout on the image gathers at the third and fourth reflectors. This criterion yielded $x = 3900$ m, which is sufficiently close to the true point of continuity for the second reflector ($x = 4000$ m). Using the estimated vertical velocity at $x = 3900$ m [$V_{P0}(x = 3900\,\text{m}, z = 800\,\text{m}) = 2316$ m/s], we estimate the parameters of the second layer with high accuracy (Figure 21).

To find the point of continuity between the second and third layers, we again perform prestack depth migrations assuming that the third layer is homogeneous and isotropic. Since the second layer is laterally heterogeneous, the migration velocities range from 2400 m/s to 3400 m/s. Applying the criterion of minimum residual moveout for the fifth and the sixth reflectors, the point of continuity was found at ($x = 5937\,\text{m}, z = 1483\,\text{m}$), where the vertical velocity is $V_{P0} = 2900$ m/s. Although

the location ($x = 5937\,\mathrm{m}, z = 1483\,\mathrm{m}$) is shifted by almost 1000 m from the true continuity point between the second and third layers, the results of the velocity analysis (Figure 22) and imaging (Figure 23) are quite satisfactory.

In the absence of borehole data, the assumption of continuous vertical velocity provides a practical way to build an anisotropic heterogeneous model for prestack migration. Depending on the complexity of the model, however, the point of continuity may be estimated with a substantial lateral shift or may not exist at all. Still, our tests show that for models without steep dips or strong lateral heterogeneity, an error in identifying the point of continuity does not distort the effective parameters V_{nmo}, k_z, $\hat{k}_x$, and η. Therefore, the migrated section would still be well focused, although the imaged reflectors would be subject to a depth stretch.

8 DISCUSSION AND CONCLUSIONS

Approximating heterogeneous VTI models by factorized blocks or layers with linear velocity variation, provides a convenient way to reconstruct anisotropic velocity fields for P-wave prestack imaging. The migration velocity analysis (MVA) algorithm introduced here estimates the anisotropic parameters and velocity gradients in each block by minimizing the residual moveout of P-wave reflection events in image gathers.

The residual moveout of both horizontal and dipping events in factorized VTI media is governed by four effective parameters – the NMO velocity V_{nmo} at the surface of the factorized block, the vertical velocity gradient k_z, the quantity $\hat{k}_x = k_x\sqrt{1+2\delta}$ that contains the lateral velocity gradient k_x and the anisotropic parameter δ, and the anellipticity parameter η. Application of our MVA method confirms the conclusion of Sarkar and Tsvankin (2002; Paper I) that stable recovery of the parameters V_{nmo}, k_z, $\hat{k}_x$, and η requires reflection moveout from at least two interfaces within each block sufficiently separated in depth.

Numerical tests indicate that the velocity-analysis algorithm yields robust estimates of the four parameters if the vertical distance between the two interfaces exceeds 1/4 of the depth of the bottom reflector. For a specific model, which may be typical of the subsurface, we also determined the minimum lateral spread in the image gathers for a stable recovery of the lateral gradient k_x. Another essential condition for stable estimation of the parameter η is either the presence of dipping interfaces (dips should exceed 25°) or acquisition of long-spread data from subhorizontal reflectors providing maximum offset-to-depth ratios of at least two.

The residual moveout on image gathers for large offset-to-depth ratios was described by a nonhyperbolic function that depends on two independent moveout parameters. Although these parameters are not directly used in the velocity analysis, their best-fit values found from semblance search give an accurate approximation for the residual moveout. The MVA is implemented in an iterative fashion, with the residual moveout minimized at each iteration step by solving a system of linear equations for the parameter updates. Since the parameter estimation is performed in the post-migrated domain, the algorithm is robust in the presence of random noise and does not lose accuracy for models with significant lateral heterogeneity and dipping structures.

The main problem in the application of P-wave velocity analysis for VTI media is that the vertical velocity V_{P0}, needed to build velocity models for depth migration, is generally unconstrained by P-wave reflection moveout (Alkhalifah and Tsvankin, 1995; Grechka et. al., 2002; Tsvankin, 2001). Also, the lateral gradient k_x is always coupled to the anisotropy coefficient δ through the parameter $\hat{k}_x = k_x\sqrt{1+2\delta}$. *A priori* knowledge of V_{P0} at any *single* point in the factorized block, however, is sufficient for estimating the true lateral gradient k_x and, therefore, reconstructing the spatially varying vertical-velocity field, as well as the Thomsen anisotropic parameters ϵ and δ.

The vertical velocity can often be estimated from borehole data using either check shots or sonic logs. If no borehole information is available, a suitable model for depth imaging can be constructed by assuming that V_{P0} is continuous across layer boundaries. Then, given the value of the vertical velocity at a single point on the surface, the entire velocity model in depth can be estimated from the residual moveout of P-wave reflection events. The examples presented in the paper demonstrate that the assumption of continuity of V_{P0} offers a practical way to build reasonably accurate anisotropic velocity models that are particularly suitable for migration codes that require a smooth velocity field. As the level of structural complexity increases, however, the migration result becomes more dependent on the lateral location of the assumed continuity point, and the adopted continuous velocity field may cause errors in the final image.

For relatively simple models with subhorizontal interfaces, the distortions related to an error in the vertical velocity are limited to a depth stretch that can vary from one layer to another. In the presence of dipping interfaces, an overstated value of V_{P0} causes the imaged ones to be larger than the true dips; if V_{P0} is understated, the imaged dips are too small. In multilayered media, a depth stretch for dipping interfaces in the overburden can distort the shape of the underlying reflectors, even if the parameters immediately above these reflectors are estimated correctly.

Still, the examples given above show that the moveout of events in image gathers is not influenced by an incorrect choice of V_{P0}, and the migrated image remains well focused as long as the algorithm yields accurate values of V_{nmo}, k_z, $\hat{k}_x$, and η. This conclusion, however, may break down if the subsurface contains interfaces

with significant dip or curvature. Then P-wave reflection moveout and, therefore, residual moveout on image gathers become dependent on the vertical velocity and the parameters ϵ and δ (Le Stunff et al., 2001; Grechka et al., 2002). For models of this type, the layer-stripping approach adopted in our MVA algorithm is not always adequate because the parameters of a given layer may remain unconstrained in the absence of reflection data from deeper interfaces (Le Stunff et al., 2001).

ACKNOWLEDGMENTS

We are grateful to members of the A(nisotropy)-Team of the Center for Wave Phenomena (CWP), Colorado School of Mines, for helpful discussions and to Ken Larner for his review of the manuscript. Partial support for this work was provided by the Chemical Sciences, Geosciences and Biosciences Division, Office of Basic Energy Sciences, U.S. Department of Energy.

References

Alkhalifah, T. and Tsvankin, I., 1995, Velocity analysis for transversely isotropic media: Geophysics, **60**,1550–1566.

Alkhalifah, T., 1997, Seismic data processing in vertically inhomogeneous TI media: Geophysics, **62**, 662–675.

Červený, V., 1972, Seismic rays and ray intensities in inhomogeneous anisotropic media: Geophys. J. R. Astr. Soc., **29**, 1–13.

Gardner, G.H.F., French, W.S., and Matzuk,T., 1974, Elements of migration and velocity analysis: Geophysics, **39**, 811–825.

Grechka, V., and Tsvankin, I., 1998, Feasibility of nonhyperbolic moveout inversion in transversely isotropic media: Geophysics, **63**, 957–969.

Grechka, V., and Tsvankin, I., 1999, 3-D moveout inversion in azimuthally anisotropic media with lateral velocity variation: Theory and a case study: Geophysics, **64**, 1202–1218.

Grechka, V., Pech, A., and Tsvankin, I., 2002, P-wave stacking-velocity tomography for VTI media: Geophys. Prosp., **50**, 151–168.

Han, B., Galikeev, T., Grechka, V., Le Rousseau, J., and Tsvankin, I., 2000, A synthetic example of anisotropic P-wave processing for a model from the Gulf of Mexico, *in* Ikelle, L., and Gangi, A., Eds., Anisotropy 2000: Fractures, converted waves and case studies: Proceedings of the Ninth International Workshop on Seismic Anisotropy (9IWSA), Soc. Expl. Geophys.

Liu, Z., 1997, An analytical approach to migration velocity analysis: Geophysics, **62**, 1238–1249.

Le Stunff, Y., and Jeannot, J.P., 1998, Pre-stack anisotropic depth imaging: 60th EAGE Conference, Extended Abstracts.

Le Stunff, Y., Grechka, V., and Tsvankin, I., 2001, Depth-domain velocity analysis in VTI media using surface P-wave data: Is it feasible?: Geophysics, **66**, 897–903.

Sarkar, D., and Tsvankin, I., 2002, Analysis of image gathers in factorized VTI media: CWP Project Review (CWP-425).

Stork, C., 1991, Reflection tomography in the post migrated domain: Geophysics, **57**, 680–692.

Thomsen, L., 1986, Weak elastic anisotropy: Geophysics, **51**, 1954–1966.

Tsvankin, I., 2001, Seismic signatures and analysis of reflection data in anisotropic media: Elsevier Science Publ. Co., Inc.

APPENDIX A: ALGORITHM FOR VELOCITY UPDATE

Following the approach suggested by Liu (1997), we design the velocity-updating algorithm to minimize the variance in the migrated depths of events in image gathers. To simplify a generally nonlinear inverse (minimization) problem, we perform the velocity analysis iteratively, with a set of linear equations being solved at each iteration. Below we discuss the velocity update performed at a single (l^{th}) step of the iterative process.

Suppose that prestack migration after the $(l-1)^{\text{th}}$ iteration of the velocity analysis resulted in the migrated depths $z_0(x_j, h_k)$ (x_j is the surface coordinate of the j^{th} image gather, and h_k is the half-offset). Then the migrated depths $z(x_j, h_k)$ after the l^{th} iteration can be represented as a linear perturbation of $z_0(x_j, h_k)$:

$$z(x_j, h_k) = z_0(x_j, h_k) + \Sigma_{i=1}^{N} \frac{\partial z_0(x_j, h_k)}{\partial \lambda_i} \Delta\lambda_i \,, \quad \text{(A1)}$$

where $\partial z_0(x_j, h_k)/\partial\lambda_i$ are the derivatives of the migrated depths with respect to the medium parameters λ_i ($i = 1, 2, 3, \ldots N$), and $\Delta\lambda_i = \lambda_i' - \lambda_i$ are the desired parameter updates. The goal of the updating procedure is to estimate $\Delta\lambda_i$ and, therefore, find the parameters λ_i' to be used for the migration after the l^{th} iteration.

The variance V of the migrated depths for a single reflection event at all offsets and image gathers is

$$V = \Sigma_{j=1}^{P} \Sigma_{k=1}^{M} \left[z(x_j, h_k) - \hat{z}(x_j)\right]^2 , \quad \text{(A2)}$$

where $\hat{z}(x_j) = (1/M)\, \Sigma_{k=1}^{M} z(x_j, h_k)$ is the average migrated depth of the event at surface coordinate x_j, P is the number of image gathers used in the velocity update, and M is the number of offsets in each image gather. The minimization at each iteration step is accomplished by searching for the parameter updates that satisfy the condition $\partial V/\partial(\Delta\lambda_r) = 0$ ($r = 1, 2, 3, \ldots N$). Subsituting equation (A1) in equation (A2), differentiating the variance with respect to the parameter updates, and

setting $\partial V/\partial(\Delta\lambda_r) = 0$ yields

$$-\Sigma_{j=1}^{P}\Sigma_{k=1}^{M}\Sigma_{i=1}^{N}(g_{jk,i}-\hat{g}_{j,i})(g_{jk,r}-\hat{g}_{j,r})\Delta\lambda_i = \Sigma_{j=1}^{P}\Sigma_{k=1}^{M}[z_0(x_j,h_k)-\hat{z}_0(x_j)](g_{jk,r}-\hat{g}_{j,r})\,, \quad \text{(A3)}$$

where $g_{jk,r} \equiv \partial z_0(x_j,h_k)/\partial\lambda_r$, $g_{jk,i} \equiv \partial z_0(x_j,h_k)/\partial\lambda_i$, and $\hat{g}_{j,i} \equiv (1/M)\Sigma_{k=1}^{M} g_{jk,i}$; all derivatives are evaluated for the medium parameters λ_i.

Equation (A3) can be rewritten in matrix form as

$$\boldsymbol{A^T A\,\Delta\lambda = A^T b}\,, \quad \text{(A4)}$$

where $\boldsymbol{A}$ is a matrix with $M \cdot P$ rows and N columns whose elements are $g_{jk,r} - \hat{g}_{j,r}$, and $\boldsymbol{b}$ is a vector with $M \cdot P$ elements defined as $z_0(x_j,h_k) - \hat{z}_0(x_j)$. $\boldsymbol{A^T A}$ is a square $N \times N$ matrix, and the vector $\boldsymbol{A^T b}$ has N elements, so the problem has been reduced to a system of N linear equations with N unknowns $\boldsymbol{\Delta\lambda}$. We solve the system (A4) using a linear conjugate gradient scheme to obtain $\boldsymbol{\Delta\lambda}$ and the updated parameters $\boldsymbol{\lambda' = \Delta\lambda + \lambda}$.

The derivatives of the depths $z(x_j,h_k)$ with respect to the medium parameters λ_i (and, therefore, the matrix $\boldsymbol{A}$) can be determined from the imaging equations (e.g., Liu, 1997; Paper I):

$$\tau_s(y,h,x,z,\vec{\lambda}) + \tau_r(y,h,x,z,\vec{\lambda}) = t(y,h)\,, \quad \text{(A5)}$$

$$\frac{\partial\tau_s(y,h,x,z,\vec{\lambda})}{\partial y} + \frac{\partial\tau_r(y,h,x,z,\vec{\lambda})}{\partial y} = \frac{\partial t(y,h)}{\partial y}\,. \quad \text{(A6)}$$

Here y is the common-midpoint location at the surface, h is the half-offset, τ_s is the traveltime from the source location x_s ($x_s = y + h$) to the diffractor location (x,z) that was obtained after prestack depth migration with the medium parameters λ_i, τ_r is the traveltime from the receiver location x_r ($x_r = y - h$) to the point (x,z), and $t(y,h)$ is the observed reflection traveltime. Note that y, x, and z depend on the medium parameters λ_i, while h is an independent variable. Because x is fixed at the surface location where a particular image gather is analyzed, however, the derivative of x with respect to λ_i is set to zero.

Differentiating equation (A5) with respect to λ_i gives

$$\left[\frac{\partial\tau_s}{\partial y} + \frac{\partial\tau_r}{\partial y}\right]\frac{dy}{d\lambda_i} + \left[\frac{\partial\tau_s}{\partial z} + \frac{\partial\tau_r}{\partial z}\right]\frac{dz}{d\lambda_i} + \left[\frac{\partial\tau_s}{\partial\lambda_i} + \frac{\partial\tau_r}{\partial\lambda_i}\right] = \frac{\partial t}{\partial y}\frac{dy}{d\lambda_i}\,. \quad \text{(A7)}$$

Taking equation (A6) into account simplifies equation (A7) to

$$\left[\frac{\partial\tau_s}{\partial z} + \frac{\partial\tau_r}{\partial z}\right]\frac{dz}{d\lambda_i} = -\frac{\partial\tau_s}{\partial\lambda_i} - \frac{\partial\tau_r}{\partial\lambda_i}\,, \quad \text{(A8)}$$

or

$$\frac{dz}{d\lambda_i} = -\left[\frac{\partial\tau_s}{\partial\lambda_i} + \frac{\partial\tau_r}{\partial\lambda_i}\right]\frac{1}{q_s + q_r}\,, \quad \text{(A9)}$$

where $q_s = \partial\tau_s/\partial z$ and $q_r = \partial\tau_r/\partial z$ are the vertical slownesses evaluated at the diffractor for the specular rays connecting the diffractor with the source and the receiver, respectively.

To find the derivatives $dz/d\lambda_i$, we perform ray tracing using the prestack-migrated image after the $(l-1)^{\text{th}}$ iteration. First, the dip of the reflector needed to define the specular reflected rays is estimated by manual picking on the image. Then, for a given diffraction point on the reflector and a fixed source-receiver offset, the specular ray is traced through two models, one of which is defined by the parameters λ_i and the other by parameters slightly deviating from λ_i (i.e., λ_i are slightly perturbed). The corresponding perturbation of the traveltime between the source and the diffractor is divided by the perturbation in λ_i to obtain $\partial\tau_s/\partial\lambda_i$, while the same quantity for the traveltime leg between the diffractor and the receiver gives $\partial\tau_r/\partial\lambda_i$. The slownesses q_r and q_s at the diffraction point are part of the output of the ray-tracing algorithm (Červený, 1972).